WWW.IJRPR.COM

International Journal of Research Publication and Reviews

Journal Homepage: www.ijrpr.com ISSN 2582-7421

Mineralogical and Geochemical Baseline Characterization using FTIR and Raman Spectroscopy of Urban Soils: A case Study from Vasai–Virar City Municipal Corporation, Maharashtra, India

Komal Kumari*, Romil Dagha, Prof. (Dr.) Tejashree V. Shanbhag

Department of Life Sciences, HSNC University, Mumbai, India- 400020

DOI : https://doi.org/10.5281/zenodo.23754434

A B S T R A C T

Urban soils integrate pedogenic, lithogenic, and anthropogenic material in proportions that are rarely characterized despite their growing relevance to urban ecosystem services, including carbon storage. This study presents a mineralogical baseline for twenty surface soil samples collected across the Vasai–Virar City Municipal Corporation (VVCMC), Maharashtra, using attenuated total reflectance Fourier-transform infrared spectroscopy (ATR-FTIR) and 785 nm Raman spectroscopy. The study shows Kaolinite and quartz were the dominant phases identified by FTIR. With a well-resolved kaolinite OH-stretching doublet (~3695/3620 cm^{-1}) present in six of twenty samples and a residual quartz Si–O–Si bending doublet (~790/685 cm^{-1}) recurring across the samples. Raman spectroscopy independently confirmed anatase (TiO_2) in nine samples and quartz in one. While a further nine samples returned no confident identification, predominantly due to CCD etalon fringing and fluorescence rather than an absence of Raman-active phases. A calcite doublet (~1415–1450/873–874 cm^{-1}) appeared in three samples. Therefore, the assemblage of dominant kaolinite, residual quartz, and accessory anatase, with no detectable feldspar or mica. It is consistent with an advanced-stage, kaolinite–quartz lateritic (ferralitic) soil derived from in situ weathering of the Deccan Trap basaltic hinterland. The use of FTIR and Raman spectroscopy proved valuable both for direct phase confirmation and for diagnosing instrument-specific data-quality limitations.

Keywords: urban soil mineralogy, ATR-FTIR, Raman spectroscopy, kaolinite, lateritic weathering, Vasai–Virar

1. Introduction

Soil mineralogy provides the lithogenic baseline against which pedogenic, biological, and anthropogenic processes in a landscape can be distinguished. However, this baseline is frequently absent for rapidly urbanizing landscapes where soil research has instead concentrated on vegetation, carbon stock, and land-cover change. The Vasai–Virar City Municipal Corporation (VVCMC) in Palghar district, Maharashtra, is one such landscape: a coastal belt spanning the localities of Naigaon, Vasai, Nalasopara, and Virar. The area has undergone rapid conversion from agricultural and mangrove-fringed land to dense urban and peri-urban development over the past two decades. While remaining underlain by the weathering products of the Deccan Trap basaltic province that dominates the regional geology of coastal Maharashtra.

Under the warm, humid, monsoon-dominated climate of this region, Deccan basalt weathers through a well-documented sequence toward kaolinite- and sesquioxide-rich residual soils, locally expressed as laterites and bauxites at more mature weathering fronts (Patel, 2022). This desilication pathway is expected to leave a predictable mineralogical signature: dominant kaolinite as the stable secondary clay phase. The residual quartz surviving as the most weathering-resistant primary silicate, and accessory titanium oxides such as anatase concentrating as other elements are progressively leached (Singh & Srivastava, 2019). Urban soils, however, are rarely purely pedogenic due to construction and demolition activity. This routinely introduces calcium- and magnesium-bearing cement and concrete residues into the near-surface soil. This can react with atmospheric and soil CO_2 to precipitate secondary calcite indistinguishable in bulk mineralogical terms from naturally occurring pedogenic carbonate (Washbourne et al., 2012). Therefore, establishing a given urban soil's mineral assemblage is purely lithogenic or carries this anthropogenic overprint is therefore a necessary first step before the soil can be used as a baseline for geochemical or carbon-cycling interpretation.

Fourier-transform infrared (FTIR) and Raman spectroscopy are complementary vibrational techniques that are individually well established for mineral identification in soils and clays, but their outputs rarely overlap completely. ATR-FTIR is a bulk, surface-averaging measurement that is highly sensitive to hydroxyl-bearing phyllosilicates and to the Si–O and C–O framework vibrations of silicates and carbonates. However, is comparatively insensitive to small, non-polar lattice modes. Raman spectroscopy, conversely, is a point measurement of whatever grain lies beneath the laser spot, and is strongly sensitive to symmetric, non-polar vibrations such as the anatase Eg mode. Moreover, it is prone to being overwhelmed by fluorescence from organic coatings and, in some instrument configurations, by charge-coupled device (CCD) etalon interference fringing that can obscure genuine mineral bands (Ryabchykov et al., 2019). Used together, the two techniques can confirm identifications and can help distinguish a genuine absence of a mineral phase from an instrumental failure to detect it. This study applies both techniques to twenty surface soil samples collected across VVCMC, with the

aims of (i) establishing the dominant mineral assemblage of the area's urban soils, (ii) evaluating the extent to which FTIR and Raman identifications corroborate one another on a sample-by-sample basis, and (iii) assessing whether the resulting assemblage is consistent with in situ lateritic weathering of the Deccan basalt hinterland or carries a detectable anthropogenic overprint.

2. Materials and Methods

Twenty surface soil samples (S1–S20) were collected from across the VVCMC area, Palghar district, Maharashtra, spanning the four constituent localities of Naigaon, Vasai, Nalasopara, and Virar. The soil is distributed across the range of vegetation and land-use settings represented in the broader field survey from which this soil subset was drawn. Samples were air-dried at room temperature, and sieved to remove coarse plant debris as well as gravel-sized fragments. No chemical pretreatment was applied, so that the measured spectra reflect the bulk mineral assemblage of each sample as collected.

2.1 Attenuated total reflectance FTIR spectroscopy

Infrared spectra were acquired on a PerkinElmer Spectrum Two spectrometer fitted with a diamond single-bounce universal ATR accessory. The range covered from 4000–450 cm^{-1} at a spectral resolution of 4 cm^{-1}, with four co-added scans per sample. Each soil sample was pressed directly against the diamond ATR crystal under a controlled applied force, and an atmospheric correction was applied automatically by the instrument software prior to spectral export. Each acquisition was evaluated against the instrument's built-in quality-check routine, baseline instability, weak or strong band saturation, excessive noise, vignetting, beam blockage, negative bands, zero-transmission artifacts, etc. Peak positions and transmittance values were extracted from the instrument's automated peak-table output for each sample and were cross-referenced against established diagnostic band positions for kaolinite, quartz, and calcite (Table 1).

Table 1. Reference vibrational band assignments used for mineral identification

Mineral phase	Technique	Diagnostic band position(s)	Vibrational assignment
Kaolinite	FTIR	~3695 and ~3620 cm^{-1} (sharp doublet)	Inner-surface and inner Al–OH stretching
Kaolinite	FTIR	~910 cm^{-1}	Al–OH bending (deformation)
Quartz	FTIR	~790 and ~685 cm^{-1} (doublet)	Si–O–Si bending
Quartz	FTIR	~465 cm^{-1}	Si–O–Si bending
Quartz	Raman	128, 206, 464 cm^{-1}	E and A_1 lattice modes (464 cm^{-1} dominant)
Anatase (TiO_2)	Raman	144, 397, 515, 639 cm^{-1}	Eg, B1g, A1g/B1g, Eg lattice modes
Calcite	FTIR	~1415–1450 and ~873–874 cm^{-1}	CO_3^{2-} asymmetric stretch and out-of-plane bend
Adsorbed/structural water	FTIR	~3375–3415 (broad) and ~1630–1638 cm^{-1}	O–H stretch and H–O–H bending
Silicate matrix (bulk)	FTIR	~994–1002 cm^{-1}	Si–O stretching envelope

2.2 Raman spectroscopy

Raman spectra were acquired using a 785 nm laser Raman spectrometer, with multiple replicate acquisitions collected per sample to assess reproducibility and to guard against single-grain sampling bias inherent to the small laser spot size. Raw spectra were baseline-corrected using an asymmetric least squares (ALS) algorithm to remove fluorescence background (Eilers & Boelens, 2005), followed by Savitzky–Golay smoothing to reduce shot noise while preserving peak shape (Savitzky & Golay, 1964). Candidate peaks were identified by automated peak detection at a minimum signal-to-noise ratio of four times the local noise floor, and every candidate peak was subsequently inspected manually against the raw, unsmoothed spectral trace to exclude instrumental artifacts. CCD etalon interference fringing and notch-filter edge effects, both of which can generate spurious, periodically spaced features that do not correspond to genuine vibrational modes (Ryabchykov et al., 2019). Mineral phases were assigned where reproducible peak positions, verified across replicate acquisitions, matched known Raman-active lattice modes of soil-relevant minerals, principally anatase, quartz, calcite, kaolinite, hematite, and goethite (Kingma & Hemley, 1994; Ohsaka et al., 1978).

2.3 Cross-technique integration

For each sample, the independently derived FTIR and Raman mineral identifications were compared directly, and the agreement or divergence between the two techniques were interpreted considering their differing measurement geometries. Specifically, the point-sampling nature of Raman versus the bulk, surface-averaging nature of ATR-FTIR, and their differing sensitivity to vibrational symmetries. Where one technique returned no confident identification, the corresponding result from the other technique was used to help distinguish a genuine absence of Raman- or infrared-active mineral content from an instrument- or sample-specific data-quality limitation.

3. Results and Discussion

3.1 FTIR assemblage

Across the twenty samples, three recurring FTIR features dominated the spectra: a hydroxyl-stretching region between approximately 3375 and 3695 cm^{-1}. A strong, broad silicate absorption envelope between approximately 994 and 1002 cm^{-1}, and a lower-wavenumber region between approximately 450 and 800 cm^{-1} carrying the diagnostic bending modes of quartz and clay. Six of the twenty samples (S1, S10, S13, S15, S16 and S19) displayed a sharp, well-resolved doublet at approximately 3693–3695 and 3619–3620 cm^{-1}. This aligns well with signature of the inner-surface and inner Al–OH stretching modes of well-ordered kaolinite. It is not produced by any other common soil clay mineral in this specific paired form (Vaculíková & Plevová, 2005). The remaining samples instead showed a single, broader hydroxyl band in the 3375–3415 cm^{-1} region without a resolvable doublet. Therefore, consistent with either a more poorly crystalline or disordered kaolinitic phase, or with a greater relative contribution of adsorbed and structural water obscuring the underlying clay OH signature.

The lower-wavenumber quartz-diagnostic doublet, classically reported near 779 and 695 cm^{-1} for well-crystallized quartz (Vaculíková & Plevová, 2005). It was recovered at a shifted position of approximately 790 and 683–691 cm^{-1} across most of the samples, accompanied in most cases by a further band near 463–465 cm^{-1} assignable to Si–O–Si bending. The doublet was fully resolved in the automated peak tables of roughly half the sample set and only partially resolved. With a single band surviving the automated peak-picking threshold, it can be a difference in relative band intensity rather than a true absence of quartz, since the strong, broad silicate stretching envelope near 994–1002 cm^{-1}. Itself consistent with overlapping clay and quartz Si–O stretching contributions, was present in every sample without exception.

A calcite-diagnostic doublet, comprising the carbonate asymmetric stretch near 1414–1450 cm^{-1} and the out-of-plane bending mode near 873–874 cm^{-1} (Vaculíková & Plevová, 2005), was identified in three samples (S4, S5, and S18). All three otherwise showing the same kaolinite/quartz-bearing clay matrix as the rest of the set. No feldspar- or mica-diagnostic bands were identified in any of the twenty peak tables, consistent with an assemblage from which primary aluminosilicates other than residual quartz have already been removed by weathering.

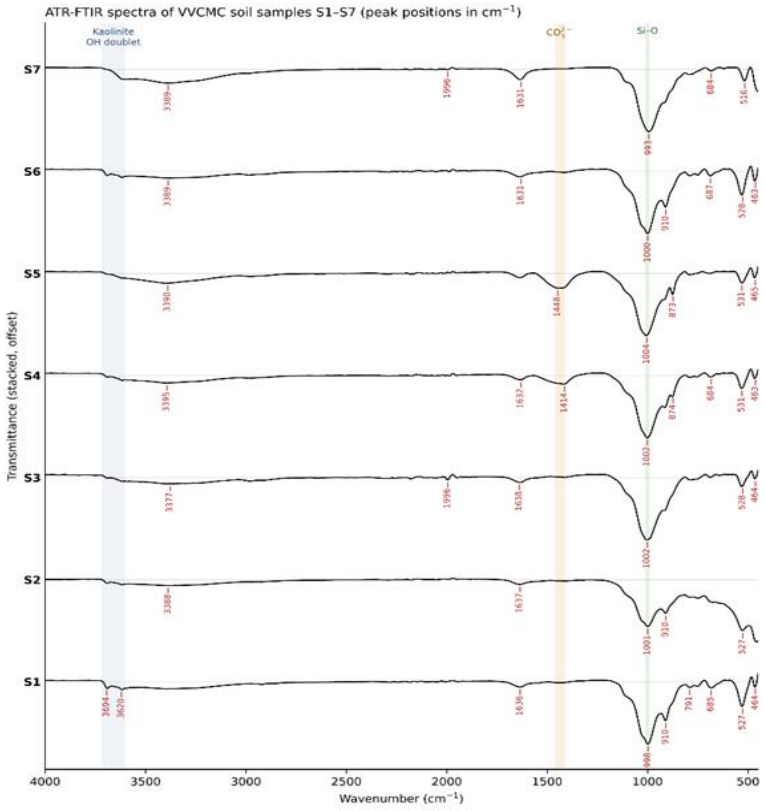


Figure 1. ATR-FTIR spectra (4000–450 cm^{-1}) of urban surface soil samples S1–S7 from VVCMC, with peak positions labelled in cm^{-1}. Shaded bands mark the kaolinite Al–OH stretching doublet (~3694/3620 cm^{-1}), the carbonate asymmetric stretch (~1414–1448 cm^{-1}), and the Si–O stretching envelope (~1000 cm^{-1}).

3.2 Raman assemblage

Raman spectroscopy independently confirmed anatase, identified by its characteristic low-wavenumber Eg lattice mode together with supporting bands in the 390–650 cm^{-1} region (Ohsaka et al., 1978), in nine of the twenty samples (S1, S3, S5, S6, S7, S10, S13, S16, and S19). It confirmed quartz, as its dominant 464 cm^{-1} A_1 symmetric Si–O–Si stretching mode (Kingma & Hemley, 1994), in one further sample (S14), with a tentative secondary quartz call in S16. The remaining nine samples (S2, S8, S9, S11, S12, S15, S17, S18, and S20) returned no confident mineral identification under the reproducibility and signal-to-noise criteria applied. Of these, the majority (S9, S12, S15, S17, and S20) were affected by a systematic CCD etalon fringing artifact associated with the wide-range acquisition protocol used for a subset of replicates. While S11 and S18 were dominated by fluorescence background sufficient to obscure any underlying Raman signal, and S2 and S8 returned low-signal-to-noise spectra without a clearly reproducible artifact explanation.

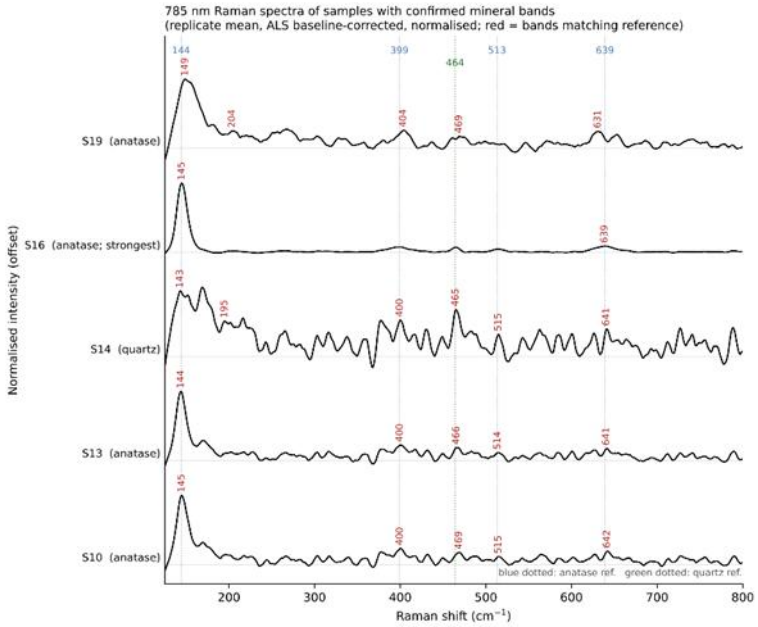


Figure 2. *785 nm Raman spectra of VVCMC soil samples with confirmed mineral bands (S10, S13, S14, S16, S19). Each trace is the mean of replicate acquisitions after asymmetric least squares baseline correction and Savitzky–Golay smoothing, normalised and offset for clarity. Dotted lines mark reference anatase bands (144, 399, 513, 639 cm^{-1}) and the quartz A_1 mode (464 cm^{-1}); red labels give the observed band positions.*

3.3 Cross-technique corroboration

The integrated, sample-by-sample comparison (Table 2) shows a consistent and informative pattern. In every sample where Raman spectroscopy confirmed anatase (S1, S10, S13, S19, and, with caveats, S3). FTIR could neither confirm nor exclude the finding directly, since anatase's diagnostic Ti–O lattice modes lie below or at the 450 cm^{-1} lower limit of this ATR-FTIR configuration. This is an expected and non-contradictory limitation of the bulk technique rather than a disagreement between methods. More informatively, four of these five anatase-bearing samples (S1, S10, S13, and S19) also carried the clearest, best-resolved kaolinite doublet and the fullest quartz doublet of the entire set. This is a pattern consistent with Raman's point measurement having sampled a discrete anatase grain embedded within a particularly well-crystallized surrounding kaolinite–quartz matrix that the bulk-averaging FTIR measurement captured independently. The clearest departure from this pattern is S16, in which Raman returned the strongest anatase signal of the entire series. While FTIR returned one of the sparsest spectra in the set, lacking both the kaolinite doublet and a fully resolved quartz doublet. This divergence is attributed to the fundamentally different sampling volumes of the two techniques: Raman's micrometre-scale laser spot can register a strong signal from a single well-formed anatase crystal regardless of the crystallinity or abundance of the surrounding bulk matrix. Whereas ATR-FTIR averages over a much larger surface area and is correspondingly more sensitive to the bulk clay content present.

Table 2. Integrated FTIR and Raman results for all twenty VVCMC soil samples

Sample	Raman identification	FTIR identification	Integrated interpretation
S1	Anatase	Kaolinite (doublet) + quartz-consistent bands	Complementary: bulk kaolinite–quartz matrix around an anatase grain
S2	No confident ID	Clay matrix (Si–O, Al–OH); no kaolinite doublet	Clay likely a weak Raman scatterer; mineralogically not empty
S3	Anatase (sample-label unresolved)	Clay + tentative quartz (low confidence; noisy spectrum)	Weak corroboration only; data-quality caveats apply
S4	Quartz	Quartz + clear carbonate doublet (1414/874 cm^{-1})	Agreement on quartz; new carbonate finding
S5	Anatase + tentative carbonate	Quartz + clear carbonate doublet (1448/873 cm^{-1})	Carbonate call strengthened from tentative to confirmed
S6	Anatase + quartz + carotenoid	Quartz + clay (Al–OH); no carbonate	Agreement on quartz; carotenoid not FTIR-visible (expected)
S7	Anatase (cleanest Raman signal)	Quartz (overtone) + highest Si–O absorption of the set	Both techniques independently flag this as the richest, cleanest sample
S8	No confident ID (low SNR)	Clay + weak/partial quartz bands	Low signal by both techniques; genuinely modest mineral content
S9	No confident ID (CCD fringing)	Clay + quartz bands, normal strength	Bulk matrix present; Raman failure attributable to instrumental artifact
S10	Anatase confirmed	Kaolinite (doublet) + full quartz doublet	Complementary; richest FTIR spectrum of the S8–S14 subset
S11	No confident ID (fluorescence)	Weak/shallow throughout; independently QC-flagged	Both instruments underperformed; treat with caution
S12	No confident ID (CCD fringing)	Clay + quartz, normal strength	Supports instrumental explanation for Raman failure
S13	Anatase confirmed	Kaolinite (doublet) + full quartz doublet	Mirrors S10; second-richest FTIR spectrum
S14	Quartz confirmed	Full quartz doublet, strong	Direct two-technique agreement
S15	No confident ID (CCD fringing)	Kaolinite + full quartz doublet + overtone (richest overall)	Strongly supports instrumental artifact, not mineral absence
S16	Anatase confirmed (strongest) + tentative quartz	Sparse clay; weak/partial quartz; no kaolinite doublet	Mismatch: strongest point-Raman anatase paired with weakest bulk matrix
S17	No confident ID (CCD fringing)	Weak throughout; independently flagged (Weak Bands)	Possibly a genuinely low-mineral-content sample
S18	No confident ID (fluorescence)	Clay + quartz + carbonate (new finding)	Carbonate/organic matrix plausibly explains fluorescence swamping
S19	Anatase + unidentified organic feature	Kaolinite (doublet) + full quartz doublet	Complementary; matches S1/S10/S13/S15 pattern
S20	No confident ID (CCD fringing)	Clay + quartz, moderate strength	Supports instrumental explanation

For the nine samples where Raman returned no confident identification, FTIR results provide a useful secondary line of evidence for distinguishing instrumental failure from genuine mineralogical poverty. In five of these samples (S9, S12, S15, S17 partially, and S20), all affected by the CCD fringing artifact, FTIR recovered an entirely ordinary, and in the case of S15 an unusually rich, kaolinite–quartz matrix. Therefore, supporting the interpretation that the Raman non-detection in these cases reflects an instrumental limitation of the wide-range acquisition protocol rather than an absence of Raman-active mineral content. By contrast, S11 and S17 showed weak, shallow absorption across their entire FTIR spectra as well, independently flagged by the spectrometer's own quality-check routine for weak bands and high noise. Therefore, both instruments converge on the same conclusion.

3.4 The carbonate anomaly

The clear calcite doublet recovered by FTIR in S4, S5, and S18 is the one feature in this dataset that sits awkwardly against the otherwise consistent kaolinite–quartz–anatase lateritic signature, since mature lateritic weathering under the humid tropical conditions implied by the rest of the assemblage is typically associated with progressive decalcification rather than carbonate accumulation (Singh & Srivastava, 2019). Two explanations are plausible and are not mutually exclusive across the three samples. A pedogenic origin, in the form of localized secondary carbonate precipitation associated with a seasonally perched water table or a calcium-enriched microsite, cannot be excluded from mineralogical evidence alone. An anthropogenic origin is, however, at least as plausible given the urban setting of all twenty sampling locations: construction and demolition debris is a well-documented source of calcium- and magnesium-bearing silicate and hydroxide residues in urban soils, which weather rapidly to precipitate secondary, pedogenic-looking calcite indistinguishable from naturally occurring carbonate by bulk vibrational spectroscopy alone (Washbourne et al., 2012). Resolving this ambiguity requires either stable-isotope or radiocarbon evidence of the kind used to distinguish geogenic from anthropogenic calcite in comparable settings, or straightforward field evidence of construction debris at the three affected sampling locations and is identified here as a priority follow-up rather than resolved by the present dataset.

The combined assemblage, dominant kaolinite as the principal secondary clay phase, residual quartz surviving as the most weathering-resistant primary silicate, accessory anatase concentrating as a residual titanium oxide, the complete absence of feldspar or mica across all twenty samples, and a localized, probably mixed pedogenic-and-anthropogenic carbonate overprint restricted to three sites, is collectively consistent with an advanced-stage, kaolinite–quartz lateritic (ferralitic) soil developed through in situ tropical weathering of the Deccan Trap basaltic hinterland underlying coastal Maharashtra. This mineralogical signature closely parallels that reported for Deccan Trap-derived laterites and bauxites elsewhere in western India, where weathered basalt progressively yields a saprolitic clay dominated by kaolinite before transitioning, at more advanced weathering fronts, toward hematite-, goethite-, and gibbsite-dominated residual laterite with anatase persisting as a minor accessory phase throughout the sequence (Patel, 2022; Singh & Srivastava, 2019). The VVCMC samples examined here correspond most closely to the kaolinite-dominant, less advanced end of this weathering continuum, rather than to a fully developed hematite–goethite laterite.

4. Conclusion

Combined ATR-FTIR and Raman spectroscopic analysis of twenty urban surface soil samples from the Vasai–Virar City Municipal Corporation reveals a consistent mineral assemblage dominated by kaolinite and residual quartz. Anatases are present as a recurring accessory phase, and no detectable feldspar or mica. This assemblage is consistent with an advanced-stage, kaolinite–quartz lateritic soil formed by in situ tropical weathering of the underlying Deccan Trap basalt, in agreement with published mineralogy from comparable Deccan-derived laterite and bauxite profiles elsewhere in western India. The two spectroscopic techniques proved strongly complementary: Raman's point-sampling geometry independently confirmed anatase that bulk ATR-FTIR cannot detect given its lower wavenumber cutoff. While bulk FTIR, in turn, demonstrated that most samples returning no confident Raman identification. Nonetheless, carry an entirely ordinary silicate matrix, indicating that most such non-detections reflect instrumental limitations, principally CCD etalon fringing and fluorescence, rather than a genuine absence of mineral content. A calcite signature restricted to three samples stands apart from the otherwise decalcified lateritic matrix and is interpreted as more likely anthropogenic, probably sourced from construction and demolition debris common to the urban setting, than purely pedogenic, though this cannot be resolved from vibrational spectroscopy alone. This dataset establishes a reproducible mineralogical baseline for VVCMC urban soils and identifies two concrete priorities for subsequent work.

Acknowledgements

The authors would like to thank the CIF Laboratory and its staff at K.C. College, HSNC University, for helping in conducting the FTIR analysis. We would also like to thank TechnoS Center of Excellence, Jaipur, for conducting the Raman Spectroscopy at their facility.

References

Patel, A., Raj, R., & Tripathi, J. K. (2022). Geochemical trends and rare Earth elements' behaviour in the recently exposed weathering profiles of the Deccan Basalts from Central India. *Journal of the Geological Society of India*, *98*(12), 1653-1660. 10.1016/j.scitotenv.2012.05.037

Eilers, P. H. C., & Boelens, H. F. M. (2005). Baseline correction with asymmetric least squares smoothing. Leiden University Medical Centre Report, 1(1), 1–26.

Kingma, K. J., & Hemley, R. J. (1994). Raman spectroscopic study of microcrystalline silica. American Mineralogist, 79(3–4), 269–273.

Ohsaka, T., Izumi, F., & Fujiki, Y. (1978). Raman spectrum of anatase, TiO_2. Journal of Raman Spectroscopy, 7(6), 321–324. https://doi.org/10.1002/jrs.1250070606

Savitzky, A., & Golay, M. J. E. (1964). Smoothing and differentiation of data by simplified least squares procedures. Analytical Chemistry, 36(8), 1627–1639. https://doi.org/10.1021/ac60214a047

Singh, B. P., & Srivastava, V. K. (2019). Petrographical, mineralogical, and geochemical characteristics of the Palaeocene lateritic bauxite deposits of Kachchh Basin, Western India. Geological Journal, 54(4), 2588–2607. https://doi.org/10.1002/gj.3313

Vaculíková, L., & Plevová, E. (2005). Identification of clay minerals and micas in sedimentary rocks. Acta Geodynamica et Geomaterialia, 2(2), 167–175.

Ryabchykov, O., Guo, S., & Bocklitz, T. (2019). Analyzing Raman spectroscopic data. *Physical Sciences Reviews*, *4*(2), 20170043. https://doi.org/10.1515/psr-2017-0043

Washbourne, C.-L., Renforth, P., & Manning, D. A. C. (2012). Investigating carbonate formation in urban soils as a method for capture and storage of atmospheric carbon. Science of the Total Environment, 431, 166–175. https://doi.org/10.1016/j.scitotenv.2012.05.037